

Short Communication

Facile Synthesis of Silicon Nanoparticles Embedded in 3D N-doped Graphene as Anode Materials for High-Performance Lithium Ion Batteries

Junli Li¹, Ruihong Li^{1,*}, Chaoke Bulin¹, Ruiguang Xing¹, Bangwen Zhang^{1,2,*}

¹ School of Material and Metallurgy, Inner Mongolia University of Science & Technology, Baotou 014010, China

² Instrumental Analysis Center, Inner Mongolia University of Science & Technology, Baotou 014010, China

*E-mail: liruihong1019@163.com, bangwenz@126.com

Received: 26 January 2017 / Accepted: 28 February 2017 / Published: 12 April 2017

The Si nanoparticle embedded in three dimensional nitrogen-doped graphene (Si-NG) composite was synthesized by a facile one-step hydrothermal method using urea as nitrogen source and vitamin C as reducing agent of graphene oxide. The composites were investigated with regard to the composition and structure by various instrumental methods and the electrochemical performances as the freestanding anode of LIBs. The results show that the Si-NG composite anode affords high storage energy and rate capability. A high discharge capacity of 1373 mAhg⁻¹ over 100 cycles is obtained at 400 mA g⁻¹, with coulombic efficiency of 98.3%. The excellent electrochemical performance is associated with high electrical conductivity of N-doped 3D graphene, short transportation path for both lithium-ions and electrons due to nanocrystallization of Si, and elastomeric space to accommodate volume changes during alloying /dealloying.

Keywords: silicon nanoparticle; Nitrogen-doped graphene; freestanding; anode; lithium-ion batteries

1. INTRODUCTION

As one of the most important devices of sustainable and recoverable energy storage, rechargeable lithium-ion batteries (LIBs) have been widely applied in portable electronics and the emerging electric vehicles [1-3]. However, the current graphite anode cannot satisfy the ever increasing demands of electric vehicles (EV) industry, and much effort has been devoted to develop the next generation of anode materials with higher energy density, and good rate performance. Among the anode materials, silicon (Si) has been regarded as the most attractive and promising anode material,

since they offer exceptionally high theoretical specific capacitance (4200 mAhg^{-1}), relative low discharge potential and the abundant resources on earth [4-6]. Despite its promise, silicon suffers from large volumetric expansion (about 400%), and low electrical conductivity and ionic diffusivity. The former would result in electrode pulverization and loss of electrical contact, and the latter restrains the achievement of a high capacity at high rates. Moreover, the formation of solid electrolyte interface (SEI) films seems to result in low columbic efficiency and a rapid fading of capacity during battery cycling [5-7]. Therefore, silicon-based anodes with high energy density and long cycle life are developed to accelerate the emergence of next generation LIBs.

To overcome these problems, one of main strategies employed in current researches is coupling Si with conductive carbonaceous materials, such as Si-carbon nanofibers, Si-carbon nanotubes, Si-amorphous carbon, and Si-graphene sheets [6-10]. Compared with other hard carbonaceous materials, two-dimensional graphene nanosheets possess higher electrical conductivity, larger specific surface area and excellent flexibility, accordingly more suitable for serving both as an elastic buffer and an electrically conductive network for the Si particles, because of its high electric conductivity, excellent chemical stability and structural flexibility [11-15]. Fu et al. [16] fabricated the Si/graphene nanocomposite electrode by the in situ magnesiothermic reduction method. A high charge capacity of 1081 mAh g^{-1} with a coulombic efficiency of 45.5% was attained in the first cycle, but the composite electrode delivered a reversible capacity of only 343 mAh g^{-1} at the current density of 8.0 A g^{-1} , exhibiting a heavy capacity loss. Z.Liu and his cooperators [17] reported carbon-coated Si nanoparticles /reduced graphene oxide anode which exhibited a good specific capacity of 800 mAh g^{-1} after 350 cycles at a current density of 2.0 A g^{-1} . However, it remains a challenge to evenly disperse Si within the graphene sheets. Thus, it is very important to obtain a stable composite with homogeneous distributed composite materials.

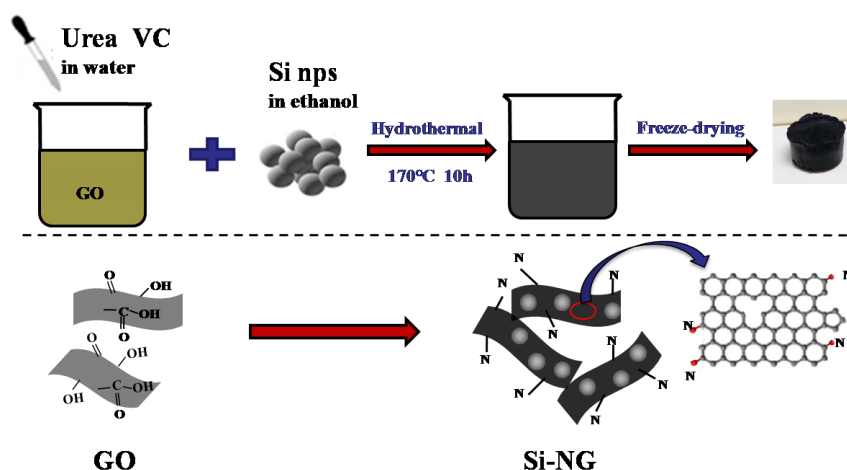
Herein, we demonstrated a facile and rapid method for the fabrication of three-dimensional (3D) Graphene-Si anodes with Si nanoparticles embedded in the nitrogen doped (N-doped) graphene framework (named as Si-NG) via one-step hydrothermal reaction. The results show that, benefiting from the N-doped graphene sheets with superior electronic conductivity, high structural flexibility and excellent mechanical strength, the as-synthesized composite shows enhanced electrochemical performances in terms of specific capacity, stable ability and rate capability when used as the Li-ion batteries anode.

2. EXPERIMENTAL

2.1. Synthesis of Si-NG composite

The synthetic route for fabrication of Si-NG composite is schematically illustrated in Scheme 1. Typically, graphene oxide (GO) was synthesized from the natural graphite via modified Hummers method [18]. The final suspension of GO is controlled at 6 mg mL^{-1} . With the assistance of ultrasonication, 60 mg Si NPs (average size $\sim 100 \text{ nm}$) were dispersed in 10 mL acetonitrile and an anionic surfactant of sodium lignosulfonate at 20 wt% of Si total weight was added to achieve stable

nano-Si dispersion. After that, the dispersion was centrifuged at 10000 rpm for 15min. After removing the supernatant, the modified nano-Si was washed several times and dissolved in ethanol. At the same time, 170 mg urea and 40 mg ascorbic acid (VC) were dissolved into deionized water by ultrasonic treatment. Both the modified nano-Si dispersion and the mixture of urea and VC were added into GO suspension. After stirring continuously for 5 h, the mixture was transferred into a stainless steel autoclave, and reacted at 170 °C for 10 h. After repeated washing with deionic water and ethanol, the 3D structural Si-NG composite was finally obtained by freeze-drying. For comparison, undoped graphene composite (Si-G) were prepared following the same procedure as the above. The obtained 3D Si-NG or Si-G composite was cut into slices with a thickness of about 1mm, which can act directly as the anodes of LIBs.



Scheme 1. Schematic illustration for synthesis of the 3D structural Si-NG composite

2.2 Characterization

The morphologies of the obtained composites were characterized by field-emission scanning electron microscopy (FE-SEM, Hitachi S-4800), and Raman spectrometer (RS, Renishaw). The crystal structure of the resultant materials was characterized by X-ray powder diffraction (XRD, PANalytical X'Pert PRO). X-ray photoelectron spectroscopy (XPS) measurements were conducted by a Kratos Axis Supra instrument with focused monochromatic Al K α radiation.

2.3 Electrochemical Measurement

CR2032 coin half-cells assembled in a glove box filled with Ar for the evaluation of electrochemical performance. The as-prepared 3D structured composite was directly employed as the working electrode without a conductive additive and binder, and the lithium foil acted as the counter and reference electrode. The electrolyte was 1M LiPF₆ dissolved in a mixture of ethylene carbonate (EC), diethyl carbonate (DEC), and dimethyl carbonate (DMC) at the ratio of 1:1:1 by volume, and the microporous polypropylene film was used as separator. Cyclic voltammetry (CV) was measured

through an electrochemical workstation (ChenhuaCHI-660E) at a scanning rate of 0.03mV s^{-1} . The galvanostatic charge/discharge tests were carried out between 0.01 and 3.0 V on a multichannel battery tester (LAND CT2001A).

3. RESULTS AND DISCUSSION

3.1. Structure and morphology of Si-NG composite

Fig.1a shows XRD patterns of nano-Si particles, GO, and the as-prepared composites. The characteristic diffraction peaks of Si-NG composite could be easily observed at about 28.4 , 47.3 , and 56.1° , corresponding to (111), (220), and (311) diffraction of Si [19-21]. The emerged broad peak at about 23° can be assigned to the (002) diffraction of disordered structure of graphene sheets [21]. It has been confirmed that the weakening and widening of graphene peak at 23° indicates successful exfoliation of graphene sheets with loose and disordered structure [22]. To further explore the structural information of graphene, Raman spectroscopy was examined and the result is shown in Fig.1b. The sharp characteristic peak centered at 520 cm^{-1} is ascribed to crystalline Si. Two peaks at 1350 and 1580 cm^{-1} correspond to the strong disorder band (D-band) and tangential mode band (G-band) of carbon, respectively [23-25]. The D-band results from structural disorder or defects in carbon materials and the G-band corresponded to the in-place stretching motion of sp^2 -bonded carbon atoms [24]. Relative intensity ratio (I_D/I_G) is generally used to evaluate the degree of disorder and defects in graphene. Compared with the ratio (I_D/I_G) of Si-G with 0.83, the Si-NG composite shows higher value of 0.94, indicating the increasing defects and structural disorder from the N-doping of graphene [26]. Moreover, it is beneficial for Li ions diffusing and for the electrolytes penetrating into the graphene sheet to react with Si nanoparticles under the existence of these defects [27].

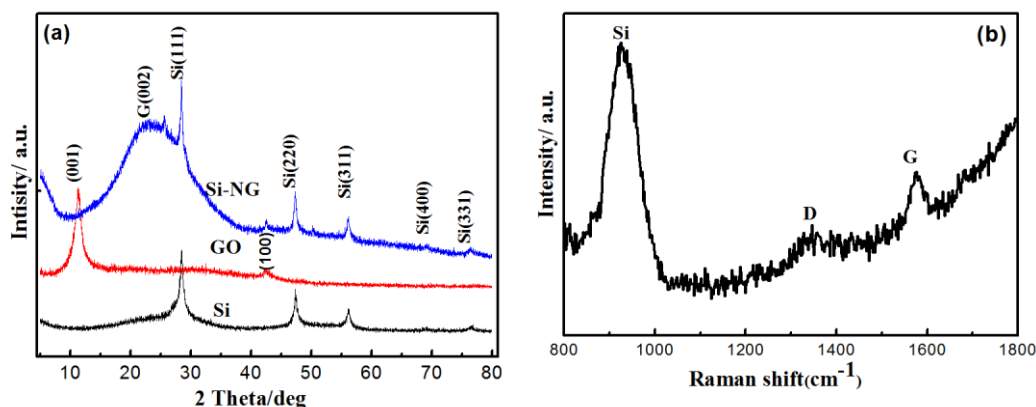


Figure 1. XRD patterns of Si, GO, and Si-NG composite (a) and Raman spectra of Si-NG composite (b)

To further detect the elemental content and chemical state of the Si-NG composite, XPS is carried out and the result is exhibited in Fig.2. In the full spectra of Si-NG (Fig. 2a), C, O, N, and Si elements coexist, which mean the success of N doping [24, 26] and Si coupling [27-29] in graphene.

From the C 1s spectrum (Fig. 2b), three single peaks centered at 284.5 eV, 285.6 eV, 286.6 eV and 289 eV are deconvoluted and assigned to C-C (C=C/C-H), C-N (C=N), C-O-C (C-OH) and O=C-OH, respectively, which indicates the existence of doped heteroatoms in the composite [26, 30]. In the Si 2p spectrum (Fig. 2c), the main peak can be resolved into Si-O (103.58 eV) and O-Si-O (104.25 eV) respectively [27, 28], and the shoulder peak at 99.21 eV corresponding to the Si 0 [27, 29, 31]. The Si-O bands, resulted from the slight oxidation of the freshly prepared Si nanoparticles, probably were entitled to some channels for Li-ions intercalation/de intercalation [29]. In addition, the formation of SiO_x thin layer could further enhance the adhesion between Si and graphene [30]. The N 1s spectrum (Fig. 2d) suggests that three types of bonded N, that is, pyridinic-N (398.1 eV), pyrrolic-N (399.7 eV), and graphitic-N (401.3 eV), contribute the sharp peak of Si-NG composite [24, 26]. As reported in previous literature, Nitrogen doping can generate more defect sites and vacancies in carbon materials, which can offer continuous transport channels for Li ions, leading to enhanced electrochemical performance of the electrode [1, 32]. The contribution of various N-doped states to the electrochemical performance can be mainly summarized as follows. The graphitic N can offer additional electrons, which can increase the conductivity of the graphene; while the pyridinic N is electrochemically active because of the lone pair of electrons which can easily conjugate with the carbon p-rings, and the pyrrolic N can improve the electron transfer [26, 30]. Therefore, the conductivity of graphene can be improved due to the graphitic N, and the excellent cycling stability may be attributed to both pyrrolic and pyridinic N in N-doped graphene nanosheets. It indicates that, the electrochemical performance of N-doped graphene wrapped Si nanoparticles will be dramatically improved compared to un-doped one.

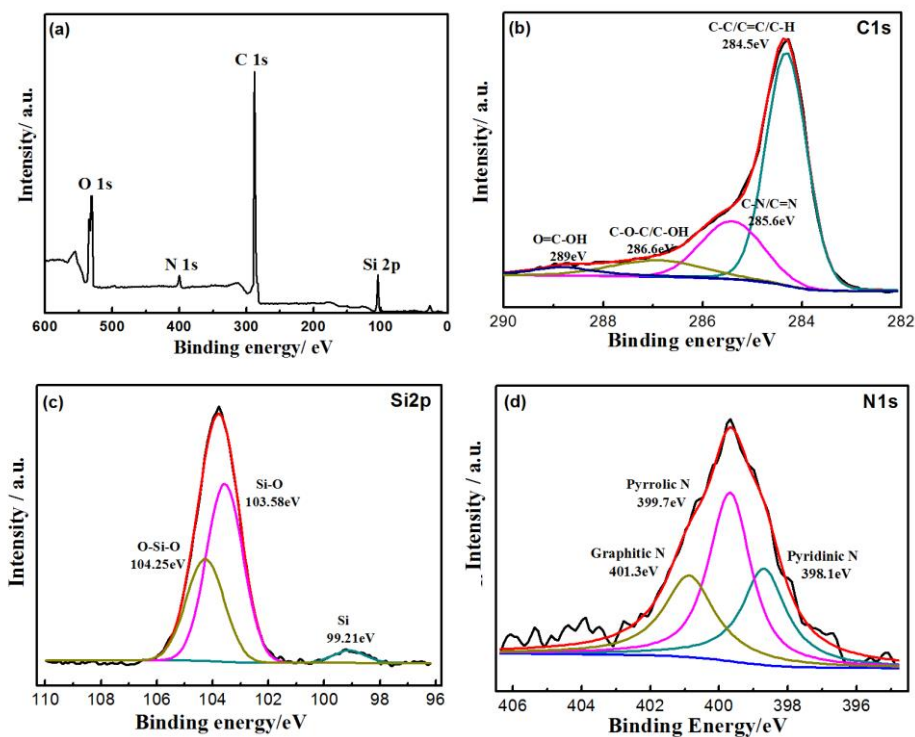


Figure 2. (a) General XPS spectrum of Si-NG composite; (b) High-resolution C1s XPS spectrum of Si-NG composite; (c) High-resolution Si2p XPS spectrum of Si-NG composite; and High-resolution N 1s XPS spectrum of Si-NG composite

Fig. 3 gives the typical morphology and elemental mapping of Si-NG composite. The obtained Si-NG composite appears cylinder-like foam (Fig. 3b), so can service as a freestanding anode. Fig. 3a and b show that Si nanoparticles are well embedded in 3D N-doped graphene network by absorbing on the surface of the graphene sheets and sandwiching between the graphene layers. As a result, the 3D Si-NG not only provides direct conductive path convenient for electrochemical reaction, but also are capable of accommodating the volume expansion of Si nanoparticles during the charge/discharge cycling [16, 33], which helps to enhance the rate capability. Furthermore, EDS mapping (Fig. 3c-f) shows the uniform distribution of C, N and Si elements, and confirms that N element is successfully doped in graphene structure.

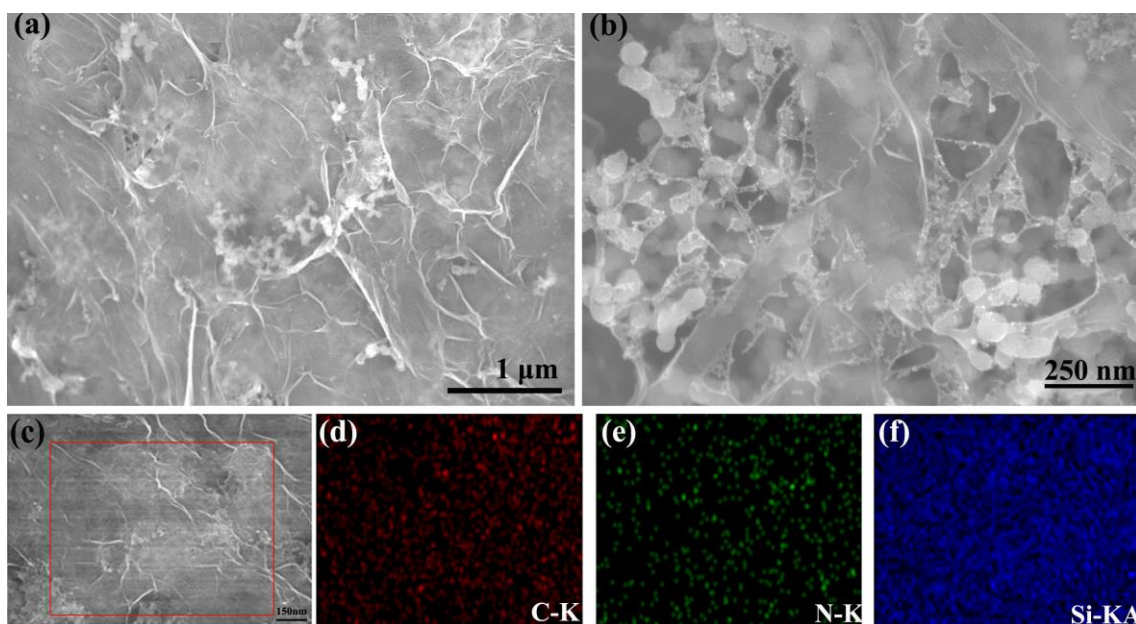


Figure 3. (a, b) SEM images and (c-f) EDS mapping of the Si-NG composite

3.2 Electrochemical properties of Si-NG composite anodes

The electrochemical behaviors of the Si-NG composite as the anode materials for Li^+ storage are characterized. Fig. 4a shows the cyclic voltammetry (CV) curves of the Si-NG anode in the first three cycles at a scanning rate of 0.03 mV s^{-1} over a voltage range of 0.01–3.0 V. In the first cycle, there is a cathodic peak at around 0.8 V, which relates to the formation of SEI layer and disappearing in subsequent cycles [3, 6, 20]. The sharp peak below 0.25 V corresponds to the conversion of crystalline Si into amorphous Li_xSi phase [29]. The anodic peak at 0.35 V is assigned to the dealloying of Li-Si alloy [27]. In the second and the third cycles, the reduction and oxidation peaks deliver an identical profile to the first one, suggesting an excellent reversible performance and good structural stability. Correspondingly, Fig. 4b depicts the galvanostatic charge/discharge curves for the Si-NG composite anode for the first three cycles at a current density of 400 mA g^{-1} . The initial charge and discharge capacities are 2066 and 1877 mAh g^{-1} , respectively, with Coulombic efficiency of 90.9%. It is noteworthy that, the reversible capacity after 3 cycles can still stabilize at around 1768 mA h g^{-1} . In addition, the discharge curves of the electrode tend to overlap and the related coulombic efficiency

rapidly increases with cycle number, indicating the high reversibility and enhanced stability of the Si-NG electrode upon cycling process. The rate performance of Si-NG composite is evaluated in Fig.4c. It shows the anode delivers a stable capacity of 1751, 1308, 1043, and 724 mAh g⁻¹ at current densities of 400, 800, 2000, and 4000 mA g⁻¹, respectively. When the current density gets back to 400 mA g⁻¹, the capacity recovers to 1420 mAh g⁻¹, indicating high reversibility and excellent rate capability of Si-NG composite. This may be attributed to the following factors [1, 6, 31, 33]. (1) The graphene as flexible loader accommodates the drastic volume variation during lithiation/delithiation. (2) nanoscale Si helps to limit the pulverization of electrode; (3) 3D structural graphene provides rapid transport paths for both the electrons and Li ions. Finally, the cyclic performance of Si-NG electrode is investigated in Fig.4d at a current density of 400 mA g⁻¹. The anode suffers to a capacity fading at the beginning of cycling; however, a reversible discharge capacity of 1373 mAh g⁻¹ is maintained after 100 cycles. These values are comparable with values reported by other research groups for Si-carbonaceous composites as Li-ion anode (see Table 1). It is obvious that the method of this work is simple, efficient and even economical, as compared to other routines. In a word, the Si-NG composite obtained here exhibits higher discharge capacity, good rate capability and cyclic stability.

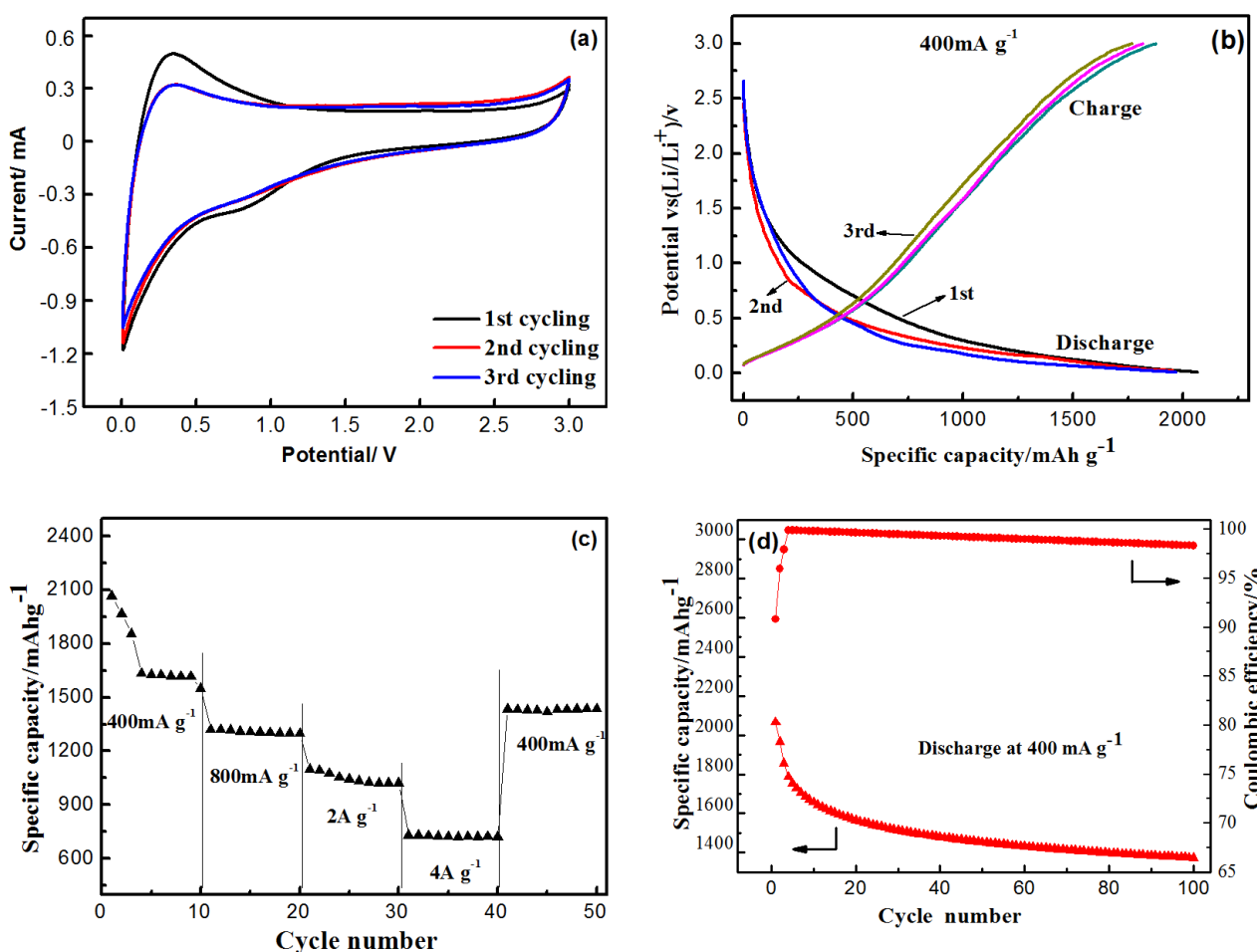


Figure 4. (a) CV curves in the first three cycles at a scanning rate of 0.03 mV s⁻¹, (b) Galvanostatic discharge/charge curves at 400 mA g⁻¹, (c) rate capability at the current densities from 0.4 to 4 A g⁻¹ and (d) cycling performance at 400 mA g⁻¹ of Si-NG composite anode

Table 1 Comparison of electrochemical properties of Si-carbonaceous composites as Li-ion anode through various synthesis methods

Products	Method	free-standing anode	Cycling performances			Ref.
			Current density (A/g)	Specific capacity (mAh/g)/ Coulombic efficiency	Cycle number	
SG-Si	Electrode coating+ sluggish heat treatment	Yes	2	1033/99.5%	2275	[3]
Si/C	Spray drying+ carbonization	No	0.5	677/97%	100	[8]
SNP@void@mG	CVD+Erosion	Yes	0.5	1287/89%	500	[9]
C@Si	Dispersing&drying+pyrolysis	No	0.21	2051/99%	100	[10]
Si/G/MWCNT	Vacuum filtration technique + radio frequency magnetron sputtering	Yes	0.1	425/90%	100	[11]
Si/G	In-situ growth+ magnesium thermal reduction	Yes	2	592/88%	300	[16]
Si/rGO/C	Alternate deposition-annealing	Yes	2	800 /99.18%	350	[17]
Si-NG	One-step hydrothermal method	Yes	0.4	1373/98.3%	100	This work

Note: SG (S-doped graphene), C (carbon), SNP (Si nanoparticle), mG(monolayer graphene), C@Si (carbon-coated Si), G (graphene), MWCNT (multiwalled carbon nanotube), rGO (reduced graphene oxide), NG (N-doped graphene).

4. CONCLUSIONS

The Si-NG composite was successfully prepared by a facile one-step hydrothermal method with a structure of 3D N-doped graphene wrapped Si nanoparticles. The well-distributed Si nanoparticles enhance the reaction activity of silicon and shorten the diffusion path of lithium ion, and the unique structure of 3D graphene frameworks helps to alleviate the volume change of Si during cycling and enable fast transport kinetics for electrons and ions. Besides, the N-doping artificially introduces the defect and vacancies in the planes of graphene, which can act as Li⁺ active sites and improve electron conductivity. As a result, the Si-NG composite exhibits high gravimetric specific capacity, better cycling performance and excellent rate capability. In particular, a high discharge capacity of 1373 mAh g⁻¹ over 100 cycles at 400 mA g⁻¹ in this system, with coulombic efficiency of 98.3%. The strategy here reported offers a promising potential in creating the freestanding composite electrodes possessing high-rate capability and long-term cyclic stability for Li-ion batteries.

ACKNOWLEDGEMENT

The authors are grateful of financial support by the National Natural Science Foundation of China (Grant No. 51164026), Natural Science Foundation of the Inner Mongolia autonomous region, china (Grant No.2015BS0512), and School of materials and metallurgy young talent incubator platform support project (Grant No.2014CY012).

References

1. C. Fu, C. Song, L. Liu, X. Xie, W. Zhao, *Int. J. Electrochem. Sci.*, 11(2016) 3876.
2. R. Raccichini, A. Varzi, S. Passerini, B. Scrosati, *Nat. Mater.*, 14 (2015) 271.
3. F.M. Hassan, R. Batmaz, J. Li, X. Wang, X. Xiao, A. Yu, Z. Chen, *Nat Commun.*, 6 (2015) 8597.

4. Y. Wang, X. Wen, J. Chen, S. Wang, *J. Power Sources*, 281 (2015) 285.
5. M. Li, J. Gu, X. Feng, H. He, C. Zeng, *Electrochim. Acta*, 164 (2015) 163.
6. Y.-Y. Kim, J.-H. Lee, H.-J. Kim, *Physica E*, 85 (2017) 223.
7. N. Liao, B. Zheng, H. Zhou, W. Xue, *Electrochim. Acta*, 156 (2015) 115.
8. W. Wang, S. Yang, *J. Alloys Compd.*, 695 (2017) 3249.
9. X. Ding, X. Liu, Y. Huang, X. Zhang, Q. Zhao, X. Xiang, G. Li, P. He, Z. Wen, J. Li, Y. Huang, *Nano Energy*, 27 (2016) 647.
10. S.-W. Park, J.-C. Kim, M.A. Dar, H.-W. Shim, D.-W. Kim, *J. Alloys Compd.*, 698 (2017) 525.
11. G. Toçoğlu, M. Hatipoğlu, F. Alaf, H. Kayış, Akbulut, *Appl. Surf. Sci.*, 389 (2016) 507.
12. Y. Wu, T. Okajima, T. Ohsaka, *Int. J. Electrochem. Sci.*, 12(2017) 1004.
13. J. Wang, C.Q. Feng, Z.Q. Sun, S.L. Chou, H.K. Liu, J.Z. Wang, *Sci. Rep.*, 4 (2014) 7030.
14. M. Shahid, N. Yesibolati, M.C. Reuter, F.M. Ross, H.N. Alshareef, *J. Power Sources*, 263 (2014) 239.
15. H. Liu, Z. Hu, R. Hu, H. Ruan, Y. Su, L. Zhang, *Int. J. Electrochem. Sci.*, 11(2016) 3376.
16. C. Fu, C. Song, L. Liu, W. Zhao, X. Xie, *Int. J. Electrochem. Sci.*, 11(2016) 154.
17. Z. Liu, P. Guo, B. Liu, W. Xie, D. Liu, D. He, *Appl. Surf. Sci.*, 396 (2017) 41.
18. H. Yu, B. Zhang, C. Bulin, R. Li R. Xing, G. xin, *Sci. Rep.*, 6(2016) 36143.
19. W. Wang, Z. Favours, R. Ionescu, R. Ye, H.H. Bay, M. Ozkan, C.S. Ozkan, *Sci. Rep.*, 5 (2015) 8781.
20. N. Liao, B. Zheng, H. Zhou, W. Xue, *Electrochim. Acta*, 156 (2015) 115.
21. L. Liu, M. An, P. Yang, J. Zhang, *Sci. Rep.*, 5 (2015) 9055.
22. N. Cuesta, A. Ramos, I. Cameán, C. Antuña, A.B. García, *Electrochim. Acta*, 155 (2015) 140.
23. Z. Zhou, W. Luo, H. Huang, S. Huang, Y. Xia, N. Zhou, Z. He, *Ceram. Int.*, 43 (2017) 99.
24. C. Liu, X. Liu, J. Tan, Q. Wang, H. Wen, C. Zhang, *J. Power Sources*, 342 (2017) 157.
25. X. Chen, Y. Huang, K. Zhang, X. Feng, S. Li, *J. Alloys Compd.*, 686 (2016) 905.
26. W. Zhao, C.M. Li, *J. Colloid Interface Sci.*, 488 (2017) 356.
27. T. Jiang, R. Zhang, Q. Yin, W. Zhou, Z. Dong, N.A. Chernova, Q. Wang, F. Omenya, M.S. Whittingham, *J. Mater. Sci.*, (2016). doi:10.1007/s10853-016-0599-8.
28. F. Jeschull, F. Lindgren, M.J. Lacey, F. Björefors, K. Edström, D. Brandell, *J. Power Sources*, 325 (2016) 513.
29. H. Kim, E.-J. Lee, Y.-K. Sun, *Mater. Today*, 17(2014) 285.
30. D. Zhou, W.-L. Song, X. Li, L.-Z. Fan, Y. Deng, *J. Alloys Compd.*, 699 (2017) 730.
31. T.L. Kulova, A.A. Mironenko, A.M. Skundin, A.S. Rudy, V.V. Naumov, D.E. Pukhov, *Int. J. Electrochem. Sci.*, 11 (2016) 1370.
32. Z. Yu, L. Wang, L. Jiang, *Ceram. Int.*, 42 (2016) 16031.
33. H. Sun, A. Varzi, V. Pellegrini, D.A. Dinh, R. Raccichini, A.E. Del Rio-Castillo, M. Prato, M. Colombo, R. Cingolani, B. Scrosati, S. Passerini, F. Bonaccorso, *Solid State Commun.*, 251 (2017) 88.